

Prediction of Long Term Restenosis Risk After Surgery in the Carotid Bifurcation by Hemodynamic and Geometric Analysis

MAURIZIO DOMANIN,^{1,2} DIEGO GALLO,³ CHRISTIAN VERGARA,⁴ PIETRO BIONDETTI,⁵ LAURA V. FORZENIGO,⁵
and UMBERTO MORBIDUCCI³

¹Department of Clinical Sciences and Community Health, Università di Milano, Milan, Italy; ²Unità Operativa di Chirurgia Vascolare, Fondazione I.R.C.C.S. Cà Granda Ospedale Maggiore Policlinico, Milan, Italy; ³PolitoBIOMed Lab, Department of Mechanical and Aerospace Engineering, Politecnico di Torino, Turin, Italy; ⁴Laboratory of Biological Structure Mechanics (LaBS), Dipartimento di Chimica, Materiali e Ingegneria Chimica “Giulio Natta”, Politecnico di Milano, Milan, Italy; and ⁵Unità Operativa di Radiologia, Fondazione I.R.C.C.S. Cà Granda Ospedale Maggiore Policlinico, Milan, Italy

(Received 2 October 2018; accepted 5 January 2019; published online 18 January 2019)

Associate Editor Lakshmi Prasad Dasi oversaw the review of this article.

Abstract—This study explored the potential of hemodynamic disturbances and geometric features to predict long-term carotid restenosis after carotid endarterectomy (CEA). Thirteen CEA for carotid diameter stenosis > 70% were performed with patch graft (PG) angioplasty in nine cases, and primary closure (PC) in four cases. MRI acquisitions within one month after CEA were used for hemodynamic and geometric characterization. Personalized computational hemodynamic simulations quantified the exposure to low and oscillatory wall shear stress (WSS). Geometry was characterized in terms of flare (the expansion at the bulb) and tortuosity. At 60 months after CEA, Doppler ultrasound (DUS) was applied for restenosis detection and intima-media thickness determination. Larger flares were associated to larger exposure to low WSS (Pearson R^2 values up to 0.38, $P < 0.05$). The two cases characterized by the highest flare and the largest low WSS exposure developed restenosis > 50% at 60 months. Linear regressions revealed associations of DUS observations of thickening with flare variables (up to $R^2 = 0.84$, $P < 0.001$), and the exposure to low (but not oscillatory) WSS ($R^2 = 0.58$, $P < 0.05$). Our findings suggest that arteriotomy repair should avoid a large widening of the carotid bulb, which is linked to restenosis *via* the generation of flow disturbances. Hemodynamics and geometry-based analyses hold potential for (1) preoperative planning, guiding the PG vs. PC clinical decision, and (2) stratifying long-term restenosis risk after CEA.

Keywords—Carotid endarterectomy, Recurrent stenosis, Computational fluid dynamics, Wall shear stress, Flare, Tortuosity.

Address correspondence to Umberto Morbiducci, PolitoBIOMed Lab, Department of Mechanical and Aerospace Engineering, Politecnico di Torino, Turin, Italy. Electronic mail: umberto.morbiducci@polito.it

Maurizio Domanin and Diego Gallo have contributed equally to this study.

ABBREVIATIONS

CB	Carotid bulb
CCA	Common carotid artery
CEA	Carotid endarterectomy
CFD	Computational fluid dynamics
DUS	Doppler ultrasound
ECA	External carotid artery
ICA	Internal carotid artery
IMT	Intima-media thickness
LSA	Low shear area
OSA	Oscillatory shear area
OSI	Oscillatory shear index
PC	Primary closure
PG	Patch graft
PSV	Peak systolic velocity
TAWSS	Time-averaged wall shear stress
WSS	Wall shear stress

INTRODUCTION

Restenosis after carotid endarterectomy (CEA) is an important complication affecting patients outcome, leading to development of cerebral symptoms or even carotid occlusion and stroke. Its overall incidence is 5.8%,³⁶ with only 8.0% of which are symptomatic patients.²⁶ In the first 2 years after surgery, restenosis is usually attributed to the development of myointimal hyperplasia,^{12,22} while intermediate (2 to 5 years) and late (> 5 years) restenosis are deemed similar to primary atherosclerotic lesions.²⁰

To minimize the risk of narrowing of the arterial lumen, the use of patch grafts (PG) for the closure of the longitudinal arteriotomy has been proposed as an alternative to primary closure (PC). Notwithstanding the recommendation for routine use of PG by current guidelines,^{8,32} doubts have been raised^{28,29,32,41} as PG involves longer cross-clamping time,⁴¹ and higher risk of neurocognitive deficits,²¹ infection, and pseudoaneurysm development.¹ A selective use for PG based on the measure of carotid diameters has also been suggested.³³

Appropriate criteria for clinical decision making regarding closure should be based on the understanding of the mechanistic processes underlying restenosis development. Among several factors, local hemodynamic disturbances are thought to contribute to the development of late restenosis after CEA.³⁴ This is supported by evidences proving a key role of low and oscillatory wall shear stress (WSS)³¹ in atherosclerosis development at the carotid bulb.^{25,31} Currently, WSS is most reliably assessed through image-based computational fluid dynamics (CFD). As an integration, or even an alternative, to CFD-based WSS estimation, previous studies proposed specific geometric attributes of the carotid bifurcation as surrogate markers of the burden of low and oscillatory WSS.^{6,27,38}

In the present study, we aim to establish whether the post-CEA hemodynamics and geometry can predict the risk of late restenosis development in a cohort of twelve patients submitted to thirteen CEA with two different closure techniques. The ultimate goal is the identification of criteria able to predict late clinical outcomes at 60 months. In perspective, the clinical translation of such criteria holds promise for guiding the choice between PG vs. PC.

METHODS

The present dataset has been previously characterized in terms of hemodynamics.¹⁰ Here we focus the analysis on the ability of hemodynamics and geometry to predict long-term restenosis with a double-blind analysis.

Ethics Statement

The study was approved by the I.R.C.C.S. Fondazione Policlinico Ethics Committee according to institutional ethics guidelines. All the patients gave their signed consent for the publication of data.

Patient Population Data

Thirteen carotid endarterectomy procedures in twelve patients with diameter stenosis of greater than 70% were evaluated by means of Doppler Ultrasound

(DUS) and magnetic resonance angiography. Stenosis of 70% or greater was defined as a peak systolic velocity (PSV) of more than 200 cm/s.²³ Further details on DUS acquisitions are provided elsewhere.¹⁰ All cases were asymptomatic, one case (8.3%) had contralateral occlusion of the internal carotid artery (ICA) and three cases (25.0%) were previously submitted to contralateral CEA. Age, sex, location of carotid stenosis, diameters of ICA, PSV, closure techniques and risk factors are listed in Table 1.

All interventions were performed under regional block anesthesia. PG angioplasty was performed in 9 cases (PG1-9) using 6 × 75 mm polyester collagen-coated patch (Ultra-thin Intervascular®, Mahwah, NJ U.S.A), tailored and distally trimmed to give a smoothly tapered transition. Cases PG1 and PG2 (right and left carotid in the same patient, respectively) were submitted to obliged PG according to the European guideline.³² In remaining cases PG was preferred to PC since ICA diameter was lower than 5.0 mm. PC was the first choice in three cases (PC1, PC3, PC4) for lesions mainly localized at the carotid bulb (CB) or with ICA luminal diameter ≥ 5.0 mm. For case PC2, initially scheduled for PG, PC was adopted for the intraoperative lack of patient's collaboration in absence of clinical sign indicating cerebral hypoperfusion or ischemia during carotid cross clamping. All patients were then submitted to DUS follow-up at 3, 24 and 60 months. All patients received regularly post-operative antiplatelet therapy (aspirin 100 mg once daily) and statins (atorvastatin 20 mg once daily).

In those cases where DUS highlighted a PSV of > 130 cm/s (indicating the presence of a diameter stenosis greater than 50%² according to the European Carotid Stenosis Trial standard), magnetic resonance angiography was conducted. Such cases were defined as cases of restenosis (according to the North American Symptomatic Carotid Endarterectomy Trial standard). Follow-ups at 3 and 24 months resulted negative to the detection of restenosis. During the follow-up period, two patients died respectively for myocardial infarction (PG4), and pancreatic carcinoma (PG8) at 36 months. After 60 months, all eligible patients were submitted to DUS follow-up. Intima-media thickness (IMT) was measured with linear 8 MHz probe and iU22 ultrasound scanner (Philips Ultrasound, Bothwell, U.S.A) and automatically extracted offline with the clinical software Qlab (Philips Ultrasound, Bothwell, U.S.A) at the following locations: ICA distal to the CB; CB; distal end of the common carotid artery (CCA), i.e., the flow divider (FD); CCA at 1 cm and 2 cm below the distal end of the CCA (FD-1 cm and FD-2 cm, respectively). No symptoms of cerebrovascular ischemia secondary to restenosis were observed in any patient during the follow-up period.

TABLE 1. Patient data.

Patient	Age (years)	Sex	Hypertension	Diabetes	Dyslipidemia	Smoker	Stenosis Location	Stenosis				
								PSV (cm/s)	CCA ϕ (mm)	BULB ϕ (mm)	ICA ϕ (mm)	ECA ϕ (mm)
PG1	65	F	Y	N	N	N	CCA, CB	375	6.00	6.00	5.00	3.80
PG2	65	F	Y	N	N	N	CB	300	6.00	5.90	5.40	4.00
PG3	81	F	Y	N	N	Y	CB, ICA	280	6.80	5.40	4.20	3.50
PG4	82	F	Y	N	N	N	CB, ICA	300	6.60	5.40	4.00	3.80
PG5	72	M	Y	Y	N	Y	ICA	372	6.69	4.83	4.50	3.97
PG6	68	F	Y	N	N	Y	CB	350	5.82	5.04	4.50	4.10
PG7	71	F	Y	N	N	N	CB, ICA	200	6.00	6.00	4.90	3.26
PG8	76	M	Y	Y	N	Y	CB	270	7.00	5.15	4.00	3.86
PG9	67	M	Y	Y	Y	Y	CB, ICA	240	6.33	6.20	4.80	2.40
PC1	81	F	Y	N	Y	Y	CB, ICA	220	7.48	7.52	4.74	4.00
PC2	79	M	N	Y	Y	N	CB, ICA	280	6.17	7.00	5.00	3.25
PC3	79	M	Y	Y	Y	Y	CCA, CB, ICA	200	8.00	8.80	7.00	5.00
PC4	61	M	Y	N	Y	N	CB	200	6.88	7.62	6.60	5.40

Age, classification of sex (*F* female; *M* male), clinical risk factors (presence of hypertension, diabetes, dyslipidemia, or smoking; *Y* yes *N* no), location of the carotid stenosis, PSV measurements at the stenosis, and diameter measurements at CCA, CB, ICA and ECA. CCA Common carotid artery, CB carotid bulb, ICA internal carotid artery, ECA external carotid artery, PSV peak systolic velocity.

From Acquisition of Clinical Images to 3D Model Reconstruction

MRI acquisitions were performed within a month after surgery with a Siemens 1.5T Avanto MR scanner, according to the following sequences and planes: Turbo Spin Echo T1 weighted axial (TR 7.50, TE 8.9, FA 144, slice 4 mm, matrix 320×224 pixels); True Fisp single shot axial (TR 873.94, TE 1.36, FA 80, slice 4 mm, matrix 256×256 pixels) and coronal (TR 1781.93, TE 1.4, FA 72, slice 3 mm, matrix 256×256 pixels) images; Turboflash 2D retrospectively electrocardiographically-gated axial images (TR 46.35, TE 1.3, FA 70, slice 6 mm, matrix 272×245 pixels). From the acquired set of images, the 3D geometry of the carotid bifurcations was reconstructed using the Vascular Modeling Toolkit software (VMTK, www.vmtk.org), as detailed elsewhere.¹⁸

Computational Fluid Dynamics

Blood was modelled as an incompressible homogeneous Newtonian fluid,³⁰ under laminar flow and rigid wall assumptions.^{11,18} Technically, the governing equations of fluid motion were numerically solved in discretized fluid domains made of tetrahedral elements, using P1 bubble-P1 finite elements and the library LifeV (<http://www.lifev.org>). In all cases, mesh size was set equal to about 0.2 cm after a mesh refinement study.¹⁸ Patient-specific flow rate waveforms were extracted from echo-color DUS at the CCA and ICA acquired within one month after surgery (i.e. at the same time as the MRI acquisition for geometry), and imposed as boundary conditions in the numerical simulations, as detailed elsewhere.¹⁸ Flow rate wave-

forms were estimated from DUS measurements by assuming a parabolic velocity profile at the CCA, and prescribed as outflow boundary conditions in the simulations applying a Lagrange multipliers-based strategy at the ICA^{11,40} to avoid assumptions on the velocity profile. At the external carotid artery (ECA) outlet section, a traction-free condition was imposed. The accuracy of the numerical results was previously verified against *in vivo* echo-color DUS measurements, as detailed elsewhere.¹⁸ From the instantaneous WSS vector distribution at the luminal surface, two WSS-based descriptors were calculated, i.e. the time-averaged WSS (TAWSS), and the oscillatory shear index (OSI).^{16,25} These hemodynamic descriptors quantify the occurrence of low and oscillatory shear stress, respectively, at the luminal surface.

For disturbed shear quantification, each carotid bifurcation was split in its constituent branches (i.e., CCA, ICA, and ECA), as detailed in previous studies.²⁷ To delimit the bifurcation region and to ensure a consistent spatial extent across all cases, the models were automatically clipped at sections located at 3, 5 and 2 radii along the CCA, ICA and ECA length,²⁷ respectively (CCA3, ICA5 and ECA2) (Fig. 1a). Data from all cases were pooled to identify the 20th percentile value of TAWSS, and 80th percentile values of OSI, to determine thresholds for disturbed shear.²⁷ These thresholds were 0.56 Pa for TAWSS and 0.03 for OSI. The burden of disturbed WSS was quantified by the surface area exposed to OSI above (TAWSS, below) the corresponding threshold value, and divided by the model surface area.¹⁶ These hemodynamic descriptors are denoted low shear area (LSA) and oscillatory shear area (OSA).

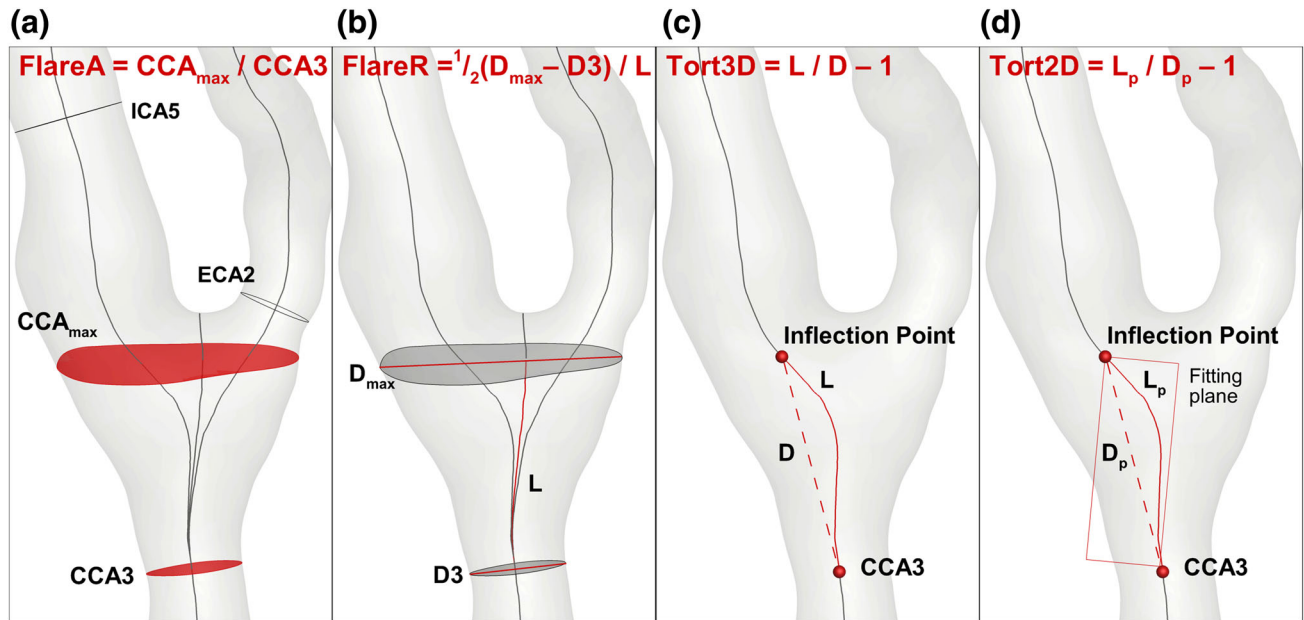


FIGURE 1. (a) CCA_{max} and $CCA3$ sections, whose areas define FlareA, are shown in red. CCA_{max} is normal to the average of the internal (ICA) and external carotid artery (ECA) centerlines. (b) FlareR was calculated as half the difference between $CCA3$ and CCA_{max} major axes (D_{max} and $D3$, respectively), divided by the distance between the sections, indicated as L in the figure. (c) The centerline segment between the $CCA3$ centerline point and the inflection point was used to calculate Tort3D as $L/D - 1$, where L is the curvilinear distance between the two points and D is the Euclidean distance between them. (d) The centerline segment between $CCA3$ and the inflection point was projected to a least-squares plane. On the projected segment on the fitting plane, the curvilinear and Euclidean distances L_p and D_p were defined to obtain Tort2D as $L_p/D_p - 1$.

Geometric Analysis

The analysis of the carotid bifurcation geometry was based on the vessel centerline, considered here the main geometric attribute of a vessel. Technically, the centerline was defined as the locus of the centers of the maximal inscribed spheres along the vessel itself.³ Centerlines were calculated automatically in VMTK as a set of discrete 3D points, which was used as input to obtain an analytical representation through 3D free-knots regression splines.^{15,17,37}

Geometric descriptors previously demonstrated to be capable of predicting the underlying “disturbed” hemodynamics were calculated^{6,27} using VMTK and Python. These descriptors quantify the bifurcation flare (i.e., the expansion), and the tortuosity of the CCA proximal to the bifurcation.⁶ Physically, a large expansion at the bifurcation promotes flow separation and in general flow disturbances,⁶ that however can be limited by a curved or tortuous upstream tract thanks to the beneficial stabilizing effect of helical flow.^{14,15} In detail, two descriptors quantifying flare were calculated. The first one, FlareA, was previously defined⁶ as the ratio between the maximum cross-sectional area at the CCA branch proximal to the flow divider (CCA_{max}) and the $CCA3$ area, to measure the expansion of the bulb with respect to the CCA (Fig. 1a). The second flare descriptor (FlareR) was previously

defined⁶ as half the difference between the two major axes of CCA_{max} and $CCA3$ (D_{max} and $D3$, respectively Fig. 1b) divided by the curvilinear distance between the two planes, to take into account the abruptness of the expansion (Fig. 1b), and that descriptors obtained from 2D planar views are easy and quick to measure in a clinical framework.

Focusing on the quantification of tortuosity, the CCA centerline was split at the so-called “inflection point”, i.e. the point proximal to the flow divider where the typically sigmoidal-shaped CCA-ICA centerline changes concavity, and at the $CCA3$ centerline point (Fig. 1c). The first tortuosity descriptor,²⁷ named Tort3D, was previously defined⁶ as:

$$\text{Tort3D} = \frac{L}{D} - 1 \quad (1)$$

where L is the curvilinear distance between the two points and D is the Euclidean distance between them (Fig. 1c). The second tortuosity descriptor (Tort2D) quantified the planar tortuosity of the CCA.⁶ The centerline between $CCA3$ and the inflection point was projected onto a plane fitting the centerline segment with a least square minimization method. Tort2D was then calculated applying the definition of tortuosity (Eq. (1)) to the projected centerline segment (Fig. 1d).

Choice of Geometric Descriptors and Comparison with Follow-Up Clinical Data

The relationship between burden of disturbed hemodynamics and the combination of flare and tortuosity descriptors was quantified by multiple linear regression analysis. The quality of the regression was evaluated with the coefficient of determination R^2 , adjusted by the number of independent predictors. The relative contribution of the predictors was determined from the standardized regression coefficients β . Then, once those geometric descriptors correlated with LSA or OSA have been identified, the ability of hemodynamic and geometric descriptors to successfully identify patient's clinical presentation at 60 months follow-up was tested. To do so, linear regression analysis was used to identify relationships between hemodynamic and geometric descriptors with the maximum IMT values found in the bifurcation region.

Successively, hemodynamic and geometric descriptors were used to assign to each patient a level of restenosis risk. In this way, patients were subdivided in three groups according to a descriptor value (i.e., low, intermediate, high), using lower and upper tertiles of the distribution of the descriptor values. This allows to define for each patient a so-called "hemodynamic restenosis risk level", when considering LSA or OSA, and a "geometric restenosis risk level", when considering the geometric descriptors. The hemodynamic or geometric restenosis risk levels were then compared with the patients' maximum IMT values, that were likewise subdivided in three groups (low, intermediate, high) according to the value using lower and upper tertiles of the distribution of the maximum IMT values across all follow-up patients.

RESULTS

Analysis of Geometry, Hemodynamics and their Relationship

The values of flare and tortuosity descriptors for PG and PC groups are reported in Table 2. As an average, PG cases presented higher values than PC of both FlareA (2.603 ± 1.422 vs. 1.329 ± 0.097) and FlareR (0.230 ± 0.114 vs. 0.161 ± 0.031). This is not unexpected as the inserted PG substitutes a portion of the endarterectomized vessel segment, which is removed in PC. Conversely, PG and PC groups presented more similar values for Tort3D (0.042 ± 0.014 vs. 0.038 ± 0.017 , respectively) and Tort2D (0.037 ± 0.015 vs. 0.036 ± 0.017 , respectively). Statistically significant differences, evaluated with a Mann-Whitney test, were found between the PG and PC groups for FlareA ($P < 0.05$).

TABLE 2. Values of geometric descriptors FlareA, FlareR, Tort3D and Tort2D for all patients within 1 month after surgery.

Patient	Flare descriptor		Tortuosity descriptor	
	FlareA	FlareR	Tort3D	Tort2D
PG1	4.952	0.455	0.067	0.064
PG2	4.800	0.385	0.052	0.044
PG3	2.266	0.188	0.034	0.022
PG4	1.855	0.175	0.033	0.032
PG5	1.437	0.132	0.043	0.039
PG6	2.047	0.153	0.053	0.046
PG7	1.310	0.181	0.045	0.043
PG8	1.455	0.148	0.028	0.026
PG9	3.305	0.253	0.020	0.014
PC1	1.320	0.180	0.021	0.019
PC2	1.197	0.178	0.034	0.032
PC3	1.418	0.115	0.061	0.059
PC4	1.383	0.171	0.037	0.035

Visualizations of WSS-based hemodynamic descriptors (Fig. 2) show that LSA and OSA are mostly localized at the bulb in correspondence of the expansion. The quantitative analysis summarized by the bar diagrams (Fig. 2, right panel) highlights that PG patients exhibit larger average values of LSA and OSA than PC patients, confirming previous reports of more unfavorable hemodynamic conditions establishing in PG than PC subjects.^{9,10} Statistically significant differences, evaluated with a Mann-Whitney test, were found between the PG and PC groups for LSA ($P < 0.05$), but not OSA ($P = 0.26$).

The interaction between the combination of flare and tortuosity vs. disturbed hemodynamics was investigated by performing multiple linear regressions over the 13 cases, with LSA or OSA as dependent variables and flare and tortuosity descriptors as independent variables (Table 3). Notwithstanding the small sample size, a direct relationship emerged between flare descriptors and LSA, as indicated by the statistically-significant R^2 and standardized correlation coefficients β ($P < 0.05$), but not OSA (Table 3).

Restenosis Risk Assessment and Comparison with Clinical Outcomes

The regression analysis between geometric and hemodynamic descriptors (Table 3) highlighted a link between flare descriptors (FlareA, FlareR) and disturbed hemodynamics (LSA). By virtue of this link, FlareA and FlareR were considered to define the "geometric restenosis risk level". For the sake of synthesis, only FlareA will be considered in the followings, while patients' subdivision based on FlareR is presented in the Supplementary Material (Supplementary Figure S1).

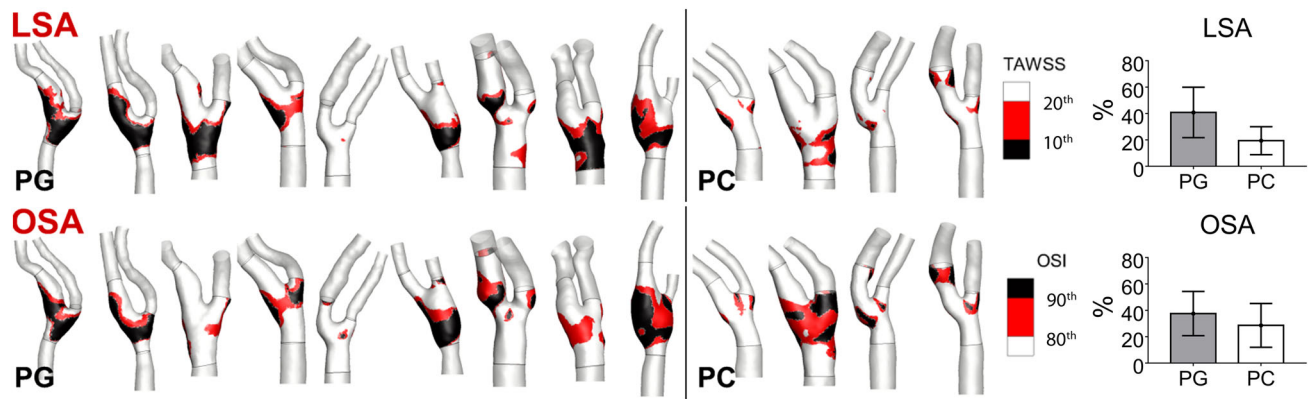


FIGURE 2. Exposure to disturbed WSS in the 13 models (PG patch graft, PC primary closure). The bifurcation region is delimited by sections CCA3, ICA5 and ECA2 and indicated by black lines in the figure. Quantitative analysis of LSA and OSA in the bifurcation region for the two groups is visualized with bar diagrams in terms of mean \pm standard deviation. Top row: exposure to low WSS as expressed by LSA. Red and black areas denote TAWSS values below respectively the 20th and 10th percentile of the pooled TAWSS distribution on all models. Bottom row: exposure to highly oscillatory WSS, as expressed by OSA. Red and black areas denote OSI values above respectively the 80th and 90th percentile of the pooled OSI distribution on all models.

TABLE 3. Multiple regression between geometry vs. hemodynamics.

	LSA			OSA		
	Adjusted R^2	β Flare	β Tortuosity	Adjusted R^2	β Flare	β Tortuosity
FlareA, Tort3D	0.3586*	0.7437*	- 0.2551	0.1323	0.5737	- 0.1995
FlareA, Tort2D	0.3840*	0.7307*	- 0.2894	0.1402	0.5586	- 0.2102
FlareR, Tort3D	0.3444*	0.7296*	- 0.2398	0.0167	0.4600	- 0.1477
FlareR, Tort2D	0.3881*	0.7395*	- 0.3096	0.0341	0.4668	- 0.1929

* $P < 0.05$.

Linear regressions revealed associations between maximum IMT and LSA ($R^2 = 0.5831$, $P = 0.006$), FlareA ($R^2 = 0.7462$, $P < 0.001$), and FlareR ($R^2 = 0.8435$, $P < 0.001$), whereas maximum IMT and OSA were not correlated ($R^2 = 0.1489$, $P = 0.241$). Scatter plots illustrating these associations are reported in the Supplementary Material (Supplementary Figure S2).

The 13 cases were then subdivided in three classes using lower and upper FlareA tertiles of the distribution of the FlareA values to define *high*, *intermediate*, and *low* “geometric restenosis risk level”. LSA and OSA distribution tertiles were similarly used to evaluate the “hemodynamic restenosis risk level” (Fig. 3). Maximum IMT values were likewise subdivided in three groups (when follow-up data were available) and used to verify the risk prediction from hemodynamic or geometric descriptors. From the subdivision presented in Fig. 3, for cases PG1 and PG2 a correspondence is evident between high FlareA, LSA and OSA values (i.e., high geometric and hemodynamic restenosis risk) with high values of maximum IMT. Moreover, FlareA and LSA correctly predicted the risk level in 7 cases out of 11. OSA correctly predicted

the risk level in 6 cases out of 11. Mispredictions were limited to contiguous groups (e.g., intermediate hemodynamic restenosis risk level but high maximum IMT value) and regarded all descriptors for PG9 and PC4, while the restenosis risk for PC2 was correctly predicted by OSA only and PG7 by FlareA only (Fig. 3). Moreover, geometric restenosis risk was overestimated for case PG5, but the hemodynamic risk for this case was correctly estimated. Interestingly, the patch in case PG5 was placed distally to the bulb, as the pre-CEA blockage was localized in the ICA (Table 1). Thus, case PG5 develop neither a primary atherosclerotic lesion nor restenosis at the bulb. This is in accordance with the low amount of disturbed WSS found at that site.

At 60 months, DUS highlighted the presence of a $> 70\%$ restenosis in PG1, and $> 50\%$ restenosis in PG2 (reminding that they belong to the same patient) (Figs. 4a and 4b). Restenosis was then confirmed by magnetic resonance angiography and intra-operative arteriography (Figs. 4c and 4d). Moreover, a clear co-localization emerged between the area exposed to low and oscillatory WSS, shown through contours of

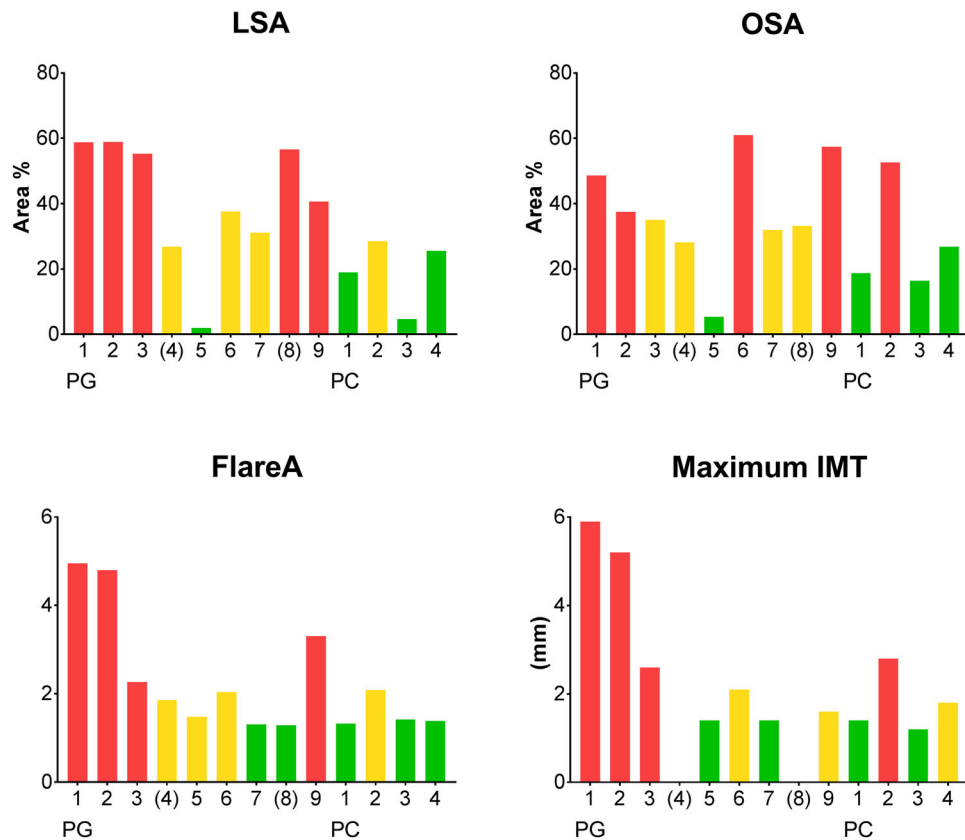


FIGURE 3. Comparison between restenosis risk assessed within 1 month after surgery by hemodynamic (LSA and OSA) and geometric (FlareA) descriptors vs. maximum IMT, measured through clinical ultrasound imaging at 60 months after surgery. Bar color represents the restenosis risk categorization: red, high risk; orange, intermediate risk; green, low risk. Top row, left panel: Restenosis risk categorization based on LSA. Top row, right panel: Restenosis risk categorization based on OSA. Bottom row, left panel: Restenosis risk categorization based on FlareA. Bottom row, right panel: Maximum IMT, expressed in mm, shows a good correspondence with LSA and FlareA data. Patients PG4 and PG8 died at three years from CEA surgery for unrelated causes, thus no follow-up data are present.

TAWSS and OSI (Figs. 4e and 4f), and the restenosis location (indicated by arrows in Fig. 4).

Clinical DUS maximum IMT measurements and velocity data at the end of the 60 months follow-up are reported in Table 4. A marked IMT (maximum IMT equal to 2.6 mm, Table 4) was observed at follow-up for PG3, which was characterized by a high geometric restenosis risk, high LSA risk but intermediate OSA risk. Marked IMT was observed at follow-up also for PG6 (maximum IMT equal to 2.1 mm, Table 4), classified as intermediate restenosis risk by its FlareA value and LSA, but high risk by OSA. Moreover, a focal restenosis process at the FD at follow-up was observed for PC2, classified as intermediate restenosis risk by its FlareA value and LSA, and high risk by OSA. In all the remaining cases (PG5, PG7, PG8, PG9, PC1, PC3, PC4), we observed a moderate IMT (Table 4).

Morphological DUS observation of the endoarterectomized regions are reported for all cases together with the TAWSS and OSI distributions at the

luminal surface to appreciate the co-localization between disturbed hemodynamics and DUS observations of myointimal thickening or new atheroma development (Fig. 5). Generally, in all cases a remarkable co-localization was observed with LSA (10 out of 11 cases), while OSA results appeared weaker (6 out of 11 cases) (Table 5).

DISCUSSION

This is the first study that (1) linked disturbed hemodynamics after CEA to verified cases of late restenosis, and (2) explored the clinical translation of such a link through surrogate geometric predictors of disturbed hemodynamics.

According to this study, hemodynamic and geometric analyses hold potential for the stratification of patients at risk for development of late restenosis. In particular the investigated descriptors LSA, OSA and flare descriptors were associated with the clinical out-

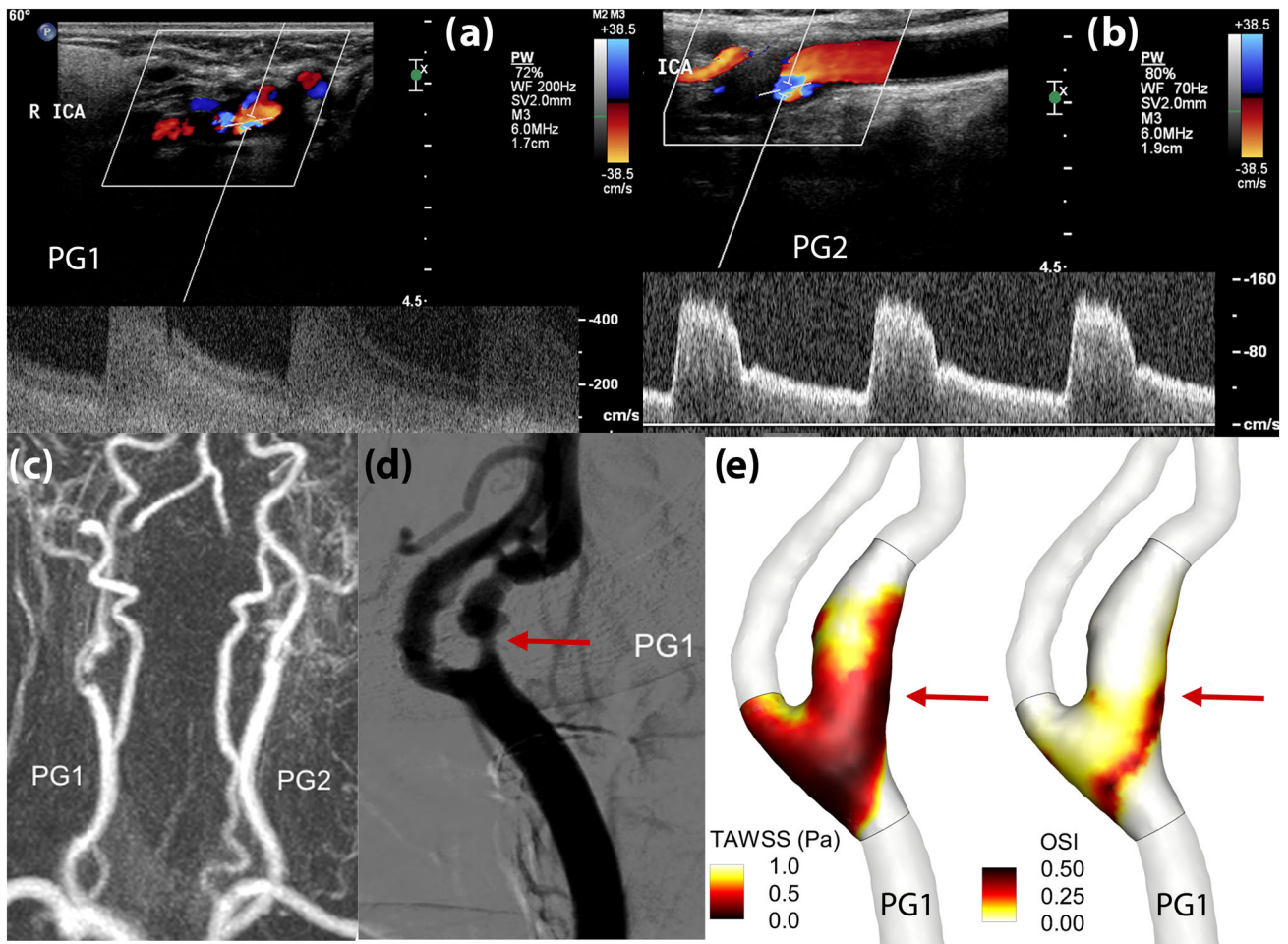


FIGURE 4. Clinical evidences of restenosis for PG1 and PG2 (note that the carotids belong to the same patient) at 60 months after surgery. Panel (a) and (b): DUS analyses for PG1 and PG2 respectively indicated a severe restenosis and PSV>130cm/s. Panel (c): magnetic resonance angiography examinations confirming the restenosis in both carotids. Panel (d): Intra-operative arteriography. Panel (e): contours of TAWSS (in Pa) and OSI for PG1 highlighted that the region where restenosis occurred was characterized by low and oscillatory WSS, as underlined by the arrows.

TABLE 4. Doppler ultrasound analysis of carotids after 60 months.

Patient	Peak systolic velocity (cm/s)	End diastolic velocity (cm/s)	Degree of restenosis (%)	IMT @ FD-2cm (mm)	IMT @ FD-1cm (mm)	IMT @ FD (mm)	IMT @ CB (mm)	IMT @ ICA (mm)	Max IMT (mm)
PG1	> 400	200	> 70	0.8	1.8	1.9	5.9	2.0	5.9
PG2	160	90	> 50	0.8	0.7	2.1	4.8	0.9	5.2
PG3	80	40	< 30	1.0	1.0	2.6	1.0	1.4	2.6
PG4	N/A	N/A	N/A	N/A	N/A	N/A	N/A	N/A	N/A
PG5	60	30	< 30	1.0	1.3	1.3	1.4	0.7	1.4
PG6	80	40	< 30	2.1	1.0	1.0	1.6	0.9	2.1
PG7	50	30	< 30	0.6	0.9	0.9	1.4	1.0	1.4
PG8	N/A	N/A	N/A	N/A	N/A	N/A	N/A	N/A	N/A
PG9	90	40	< 30	1.0	1.6	1.0	0.8	1.3	1.6
PC1	90	35	< 30	0.9	0.9	0.9	0.9	0.9	1.4
PC2	70	35	< 30	0.9	1.4	2.8	1.3	0.8	2.8
PC3	80	40	< 30	0.7	0.8	0.9	0.9	0.6	1.2
PC4	60	40	< 30	0.6	0.7	1.8	0.8	0.6	1.8

Velocities expressed in cm/s, IMT measurements in mm measured at the bifurcation level (flow divider FD), CCA at 2cm and 1cm proximal to the FD (FD-2cm and FD-1cm), at the CB, at the ICA downstream of the CB, and maximum IMT.

IMT Intima-media thickness, CCA common carotid artery, CB carotid bulb, ICA internal carotid artery, N/A not available.

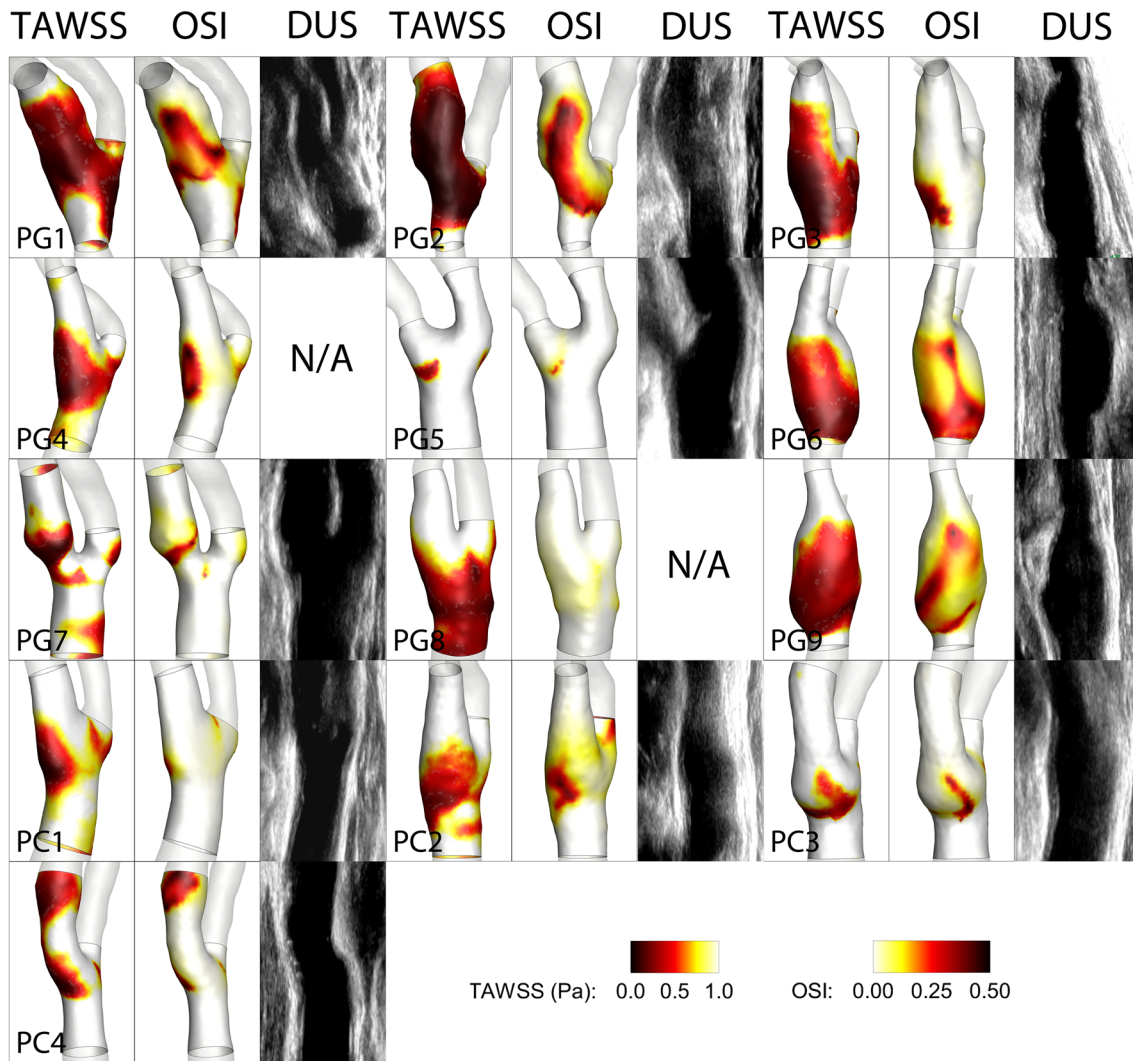


FIGURE 5. Contour maps of low and oscillatory WSS within 1 month after surgery, as indicated by TAWSS (Pa) and OSI, are shown together with follow up DUS images at 60 months, showing carotid IMT. In general, there is correspondence between low and oscillatory WSS regions and maximum IMT regions.

TABLE 5. Location of the maximum IMT region and correspondence between the co-localization of maximum IMT with LSA and OSA.

Patient	Location maximum IMT	LSA co-localization	OSA co-localization
PG1	CB/ICA	High	High
PG2	CB/ICA	High	High
PG3	CCA	High	High
PG4	N/A	N/A	N/A
PG5	CCA	High	Moderate
PG6	CCA	High	Moderate
PG7	CB/ICA	Moderate	Moderate
PG8	N/A	N/A	N/A
PG9	CCA/CB	High	Moderate
PC1	CB	High	Low
PC2	CCA/CB	High	High
PC3	CB	High	High
PC4	CB/ICA	High	High

CCA Common carotid artery, CB carotid bulb, ICA internal carotid artery, ECA external carotid artery, N/A not available.

come at 60 months follow-up. As presented in Table 3 and in the Supplementary Material, FlareR gave comparable results as FlareA in terms of LSA and OSA prediction and geometric risk subdivision. This was not known *a priori* and might offer a practical way to measure the geometric restenosis risk, as the 2D planar views of the major axes of CCA_{max} and CCA3 could be sufficient to measure FlareR. Furthermore, the present CFD analysis based on LSA and OSA quantification allowed us also to predict with good approximation the location of maximum IMT, regardless of its severity. The differences in the association between clinical outcomes (maximum IMT) and LSA or OSA suggest the possibility of different vascular responses to low vs. oscillatory WSS,³⁹ consistently with a recent *in vivo* study on hemodynamic factors in early atherosclerosis at the carotid bifurcation.¹³

The underlying mechanisms for the development of carotid restenosis after CEA are still being defined. Among the involved risk factors, the establishment of flow disturbances at the bifurcation has been often interpreted by the surgeons as harbinger of potential complications.⁵ Several investigations focused at hemodynamic alterations consequent to variations of carotid bifurcation geometry after CEA. Kamenskiy *et al.* observed wider areas of high OSI as a consequence of the abrupt diameter's transition from PG level to the native artery after PG insertion, consistently with the idea of flare promoting disturbed WSS.²⁴ Harloff *et al.* investigating carotid bifurcation of previously high-grade ICA stenosis, reported that eversion CEA tends to restore WSS to physiological values.¹⁹ Domanin *et al.* observed higher values of OSI in patients submitted to CEA when PG was inserted with respect to PC, both in obliged and selective use of PG based on the measures of the ICA or the proximal localization of the plaque.¹⁰ A virtual comparative hemodynamic analysis, explored by virtually performing PG or PC in the same carotid geometry, did not highlight disadvantages for the PC choice, in terms of hemodynamics.⁹

Surrogate markers for disturbed WSS have been proposed based on specific geometric attributes of the carotid artery, by virtue of their influence on local flow patterns.^{27,35} Bijari *et al.* demonstrated that flare and proximal CCA curvature are independent predictors of LSA and OSA⁶ and wall thickness at the carotid bulb.⁷ Archie observed that PG insertion resulted in CB geometric modifications with respect to the pre-CEA geometry, with an increase of the CB length, and a change of CB shape from elliptical to round.⁴ Here,

flare emerged as significant predictor of exposure to disturbed hemodynamics, recapitulating the detrimental effect of flare in promoting disturbed WSS.^{6,27} These findings are widened by the association between flare and long-term clinical outcomes, supporting that the introduction of a large and sudden expansion²² should be avoided as it potentially leads to abnormal responses of the endarterectomised arterial wall. This is particularly true in obliged PG arteriotomy repair strategies. Furthermore, the inverse relative contribution of tortuosity to disturbed hemodynamics (as indicated by the negative standardized coefficients in Table 3, although not significant) summarized the beneficial effect of inlet tortuosity in mitigating WSS disturbances.¹⁴

It is worth noting that previous studies demonstrated the reproducibility of the geometric characterization of the carotid bifurcation,⁴⁰ that was performed here automatically. Therefore, the quantitative geometric characterization described here could be easily and robustly obtained from imaging data, and employed at a large scale for explorative studies, clinical trials and ultimately clinical routine. In this sense, geometric analysis based on flare could be easily integrated in a surgical planning pipeline to virtually explore post-operative scenarios, providing useful indications on a case by case basis about (1) the best arteriotomy repair strategy (e.g., PG vs. PC), and (2) the best follow up strategy.

Limitations and Future Developments

Limitations are related to the small sample size, although sufficient for statistical significant correlations to emerge, to the lack of randomization, and to the absence of any analysis of biologic or systemic risk factors potentially involved in the mechanisms of restenosis.

Although these factors are needed to fully capture the total restenosis risk, we focus here on local hemodynamics risk factors and their ability to identify cases at greater susceptibility for restenosis development. Furthermore, in general computational hemodynamics suffers from uncertainties (e.g., reconstruction errors), and assumptions (e.g., Newtonian viscosity, rigid walls, as widely discussed elsewhere³⁸), that might influence the relationships described in the present study. Additionally, no information about the extension of the region subject to CEA surgical intervention (either with PG or PC) can be extracted from the imaging data.

As a consequence of the aforementioned limitations, the ability of geometry and hemodynamics to identify individuals at greater risk of developing restenosis will need to be confirmed in a prospective trial. Therefore, further adequately powered investigations are warranted.

CONCLUSIONS

The findings of this study suggest that the closure of the arteriotomy after CEA should avoid creating an excessively large widening of the carotid bulb which is linked to restenosis *via* the generation of flow disturbances. Hemodynamics and geometry analyses after CEA holds potential for the stratification of patients at risk for development of late restenosis. In a clinical framework, geometric analysis based on flare can be obtained by DUS or radiological imaging during clinical assessments in a convenient, fast and relatively easy way in a time frame compatible with clinical procedures. The presented approach could contribute to a deeper understanding of the hemodynamics-driven processes underlying restenosis development, potentially guiding the PG vs. PC clinical decision.

ELECTRONIC SUPPLEMENTARY MATERIAL

The online version of this article (<https://doi.org/10.1007/s10439-019-02201-8>) contains supplementary material, which is available to authorized users.

ACKNOWLEDGMENTS

The Authors would like to thank the technical assistance of Paola Tasso and David Iommi, and the fruitful discussion with Prof. David A. Steinman.

REFERENCES

- ¹Abdelhamid, M. F., M. L. Wall, and R. K. Vohra. Carotid artery pseudoaneurysm after carotid endarterectomy: case series and a review of the literature. *Vasc. Endovasc. Surg.* 43:571–577, 2009.
- ²AbuRahma A. F., P. Stone, S. Deem, L. S. Dean, T. Keiffer and E. Deem. Proposed duplex velocity criteria for carotid restenosis following carotid endarterectomy with patch closure. *J. Vasc. Surg.* 50: 286–291, 291 e281–282, 2009; discussion 291.
- ³Antiga, L., M. Piccinelli, L. Botti, B. Ene-Iordache, A. Remuzzi, and D. A. Steinman. An image-based modeling framework for patient-specific computational hemodynamics. *Med. Biol. Eng. Comput.* 46:1097–1112, 2008.
- ⁴Archie, J. P. Geometric dimension changes with carotid endarterectomy reconstruction. *J. Vasc. Surg.* 25:488–498, 1997.
- ⁵Bandyk, D. F., H. W. Kaebnick, M. B. Adams, and J. B. Towne. Turbulence occurring after carotid bifurcation endarterectomy—a harbinger of residual and recurrent carotid stenosis. *J. Vasc. Surg.* 7:261–274, 1988.
- ⁶Bijari, P. B., L. Antiga, D. Gallo, B. A. Wasserman, and D. A. Steinman. Improved prediction of disturbed flow via hemodynamically-inspired geometric variables. *J. Biomech.* 45:1632–1637, 2012.
- ⁷Bijari, P. B., B. A. Wasserman, and D. A. Steinman. Carotid bifurcation geometry is an independent predictor of early wall thickening at the carotid bulb. *Stroke* 45:473–478, 2014.
- ⁸Brott, T. G., J. L. Halperin, S. Abbara, J. M. Bacharach, J. D. Barr, R. L. Bush, C. U. Cates, M. A. Creager, S. B. Fowler, G. Friday, V. S. Hertzberg, E. B. McCliff, W. S. Moore, P. D. Panagos, T. S. Riles, R. H. Rosenwasser, and A. J. Taylor. ASA/ACCF/AHA/AANN/AANS/ACR/ASNR/CNS/SAIP/SCAI/SIR/SNIS/SVM/SVS guideline on the management of patients with extracranial carotid and vertebral artery disease: executive summary. A report of the American College of Cardiology Foundation/American Heart Association Task Force on Practice Guidelines, and the American Stroke Association, American Association of Neuroscience Nurses, American Association of Neurological Surgeons, American College of Radiology, American Society of Neuroradiology, Congress of Neurological Surgeons, Society of Atherosclerosis Imaging and Prevention, Society for Cardiovascular Angiography and Interventions, Society of Interventional Radiology, Society of NeuroInterventional Surgery, Society for Vascular Medicine, and Society for Vascular Surgery. *Circulation* 124:489–532, 2011.
- ⁹Domanin, M., D. Bissacco, D. Le Van, and C. Vergara. Computational fluid dynamic comparison between patch-based and primary closure techniques after carotid endarterectomy. *J. Vasc. Surg.* 67:887–897, 2018.
- ¹⁰Domanin, M., A. Buora, F. Scardulla, B. Guerciotti, L. Forzenigo, P. Biondetti, and C. Vergara. Computational fluid-dynamic analysis after carotid endarterectomy: patch graft versus direct suture closure. *Ann. Vasc. Surg.* 44:325–335, 2017.
- ¹¹Formaggia, L., J. F. Gerbeau, F. Nobile, and A. Quarteroni. Numerical treatment of defective boundary conditions for the Navier-Stokes equations. *Siam J. Numer. Anal.* 40:376–401, 2002.
- ¹²Frericks, H., J. Kievit, J. M. van Baalen, and J. H. van Bockel. Carotid recurrent stenosis and risk of ipsilateral stroke: a systematic review of the literature. *Stroke* 29:244–250, 1998.
- ¹³Gallo, D., P. B. Bijari, U. Morbiducci, Y. Qiao, Y. J. Xie, M. Etesami, D. Habets, E. G. Lakatta, B. A. Wasserman, and D. A. Steinman. Segment-specific associations between local haemodynamic and imaging markers of early atherosclerosis at the carotid artery: an in vivo human study. *J. R. Soc. Interface* 15:20180352, 2018.
- ¹⁴Gallo, D., D. A. Steinman, P. B. Bijari, and U. Morbiducci. Helical flow in carotid bifurcation as surrogate marker of exposure to disturbed shear. *J. Biomech.* 45:2398–2404, 2012.
- ¹⁵Gallo, D., D. A. Steinman, and U. Morbiducci. An insight into the mechanistic role of the common carotid artery on

- the hemodynamics at the carotid bifurcation. *Ann. Biomed. Eng.* 43:68–81, 2015.
- ¹⁶Gallo, D., D. A. Steinman, and U. Morbiducci. Insights into the co-localization of magnitude-based versus direction-based indicators of disturbed shear at the carotid bifurcation. *J. Biomech.* 49:2413–2419, 2016.
- ¹⁷Gallo, D., O. Vardoulis, P. Monney, D. Piccini, P. Antiochos, J. Schwitter, N. Stergiopoulos, and U. Morbiducci. Cardiovascular morphometry with high-resolution 3D magnetic resonance: first application to left ventricle diastolic dysfunction. *Med. Eng. Phys.* 47:64–71, 2017.
- ¹⁸Guerciotti, B., C. Vergara, L. Azzimonti, L. Forzenigo, A. Buora, P. Biondetti, and M. Domanin. Computational study of the fluid-dynamics in carotids before and after endarterectomy. *J. Biomech.* 49:26–38, 2016.
- ¹⁹Harloff, A., S. Berg, A. J. Barker, J. Schollhorn, M. Schumacher, C. Weiller, and M. Markl. Wall shear stress distribution at the carotid bifurcation: influence of eversion carotid endarterectomy. *Eur. Radiol.* 23:3361–3369, 2013.
- ²⁰Hellings, W. E., F. L. Moll, J. P. de Vries, P. de Bruin, D. P. de Kleijn, and G. Pasterkamp. Histological characterization of restenotic carotid plaques in relation to recurrence interval and clinical presentation: a cohort study. *Stroke* 39:1029–1032, 2008.
- ²¹Heyer, E. J., R. Sharma, A. Rampersad, C. J. Winfree, W. J. Mack, R. A. Solomon, G. J. Todd, P. C. McCormick, J. G. McMurtry, D. O. Quest, Y. Stern, R. M. Lazar, and E. S. Connolly. A controlled prospective study of neuropsychological dysfunction following carotid endarterectomy. *Arch. Neurol.* 59:217–222, 2002.
- ²²Imparato, A. M. The role of patch angioplasty after carotid endarterectomy. *J. Vasc. Surg.* 7:715–716, 1988.
- ²³Jahromi, A. S., C. S. Cina, Y. Liu, and C. M. Clase. Sensitivity and specificity of color duplex ultrasound measurement in the estimation of internal carotid artery stenosis: a systematic review and meta-analysis. *J. Vasc. Surg.* 41:962–972, 2005.
- ²⁴Kamenskiy, A. Computational fluid dynamic comparison between patch-based and primary closure techniques after carotid endarterectomy. *J. Vasc. Surg.* 67:897–898, 2018.
- ²⁵Ku, D. N., D. P. Giddens, C. K. Zarins, and S. Glagov. Pulsatile flow and atherosclerosis in the human carotid bifurcation. Positive correlation between plaque location and low oscillating shear stress. *Arteriosclerosis* 5:293–302, 1985.
- ²⁶Kumar, R., A. Batchelder, A. Saratzis, A. F. AbuRahma, P. Ringleb, B. K. Lal, J. L. Mas, M. Steinbauer, and A. R. Naylor. Restenosis after carotid interventions and its relationship with recurrent ipsilateral stroke: a systematic review and meta-analysis. *Eur. J. Vasc. Endovasc. Surg.* 53:766–775, 2017.
- ²⁷Lee, S. W., L. Antiga, J. D. Spence, and D. A. Steinman. Geometry of the carotid bifurcation predicts its exposure to disturbed flow. *Stroke* 39:2341–2347, 2008.
- ²⁸Maertens, V., H. Maertens, M. Kint, C. Coucke, and Y. Blomme. Complication rate after carotid endarterectomy comparing patch angioplasty and primary closure. *Ann. Vasc. Surg.* 30:248–252, 2016.
- ²⁹Malas, M., N. O. Glebova, S. E. Hughes, J. H. Voeks, U. Qazi, W. S. Moore, B. K. Lal, G. Howard, R. Llinas, and T. G. Brott. Effect of patching on reducing restenosis in the carotid revascularization endarterectomy versus stenting trial. *Stroke* 46:757–761, 2015.
- ³⁰Morbiducci, U., D. Gallo, D. Massai, R. Ponzini, M. A. Deriu, L. Antiga, A. Redaelli, and F. M. Montevecchi. On the importance of blood rheology for bulk flow in hemodynamic models of the carotid bifurcation. *J. Biomech.* 44:2427–2438, 2011.
- ³¹Morbiducci, U., A. M. Kok, B. R. Kwak, P. H. Stone, D. A. Steinman, and J. J. Wentzel. Atherosclerosis at arterial bifurcations: evidence for the role of haemodynamics and geometry. *Thromb. Haemost.* 115:484–492, 2016.
- ³²Naylor, A. R., J. B. Ricco, G. J. de Borst, S. Debus, J. de Haro, A. Halliday, G. Hamilton, J. Kakisis, S. Kakkos, S. Lepidi, H. S. Markus, D. J. McCabe, J. Roy, H. Sillesen, J. C. den van Berg, F. Vermassen, C. Esvs Guidelines, P. Kolh, N. Chakfe, R. J. Hinchliffe, I. Koncar, J. S. Lindholt, M. Vega de Ceniga, F. Verzini, R. Esvs Guideline, J. Archie, S. Bellmunt, A. Chaudhuri, M. Koelemay, A. K. Lindahl, F. Padberg, and M. Venermo. Editor's choice—management of atherosclerotic carotid and vertebral artery disease: 2017 Clinical Practice Guidelines of the European Society for Vascular Surgery (ESVS). *J. Vasc. Endovasc. Surg.* 55:3–81, 2018.
- ³³Ouriel, K., and R. M. Green. Clinical and technical factors influencing recurrent carotid stenosis and occlusion after endarterectomy. *J. Vasc. Surg.* 5:702–706, 1987.
- ³⁴Pasterkamp, G., D. P. de Kleijn, and C. Borst. Arterial remodeling in atherosclerosis, restenosis and after alteration of blood flow: potential mechanisms and clinical implications. *Cardiovasc. Res.* 45:843–852, 2000.
- ³⁵Phan, T. G., R. J. Beare, D. Jolley, G. Das, M. Ren, K. Wong, W. Chong, M. D. Sinnott, J. E. Hilton, and V. Srikanth. Carotid artery anatomy and geometry as risk factors for carotid atherosclerotic disease. *Stroke* 43:1596–1601, 2012.
- ³⁶Rerkasem, K., and P. M. Rothwell. Systematic review of randomized controlled trials of patch angioplasty versus primary closure and different types of patch materials during carotid endarterectomy. *Asian J. Surg.* 34:32–40, 2011.
- ³⁷Sangalli, L. M., P. Secchi, S. Vantini, and A. Veneziani. Efficient estimation of three-dimensional curves and their derivatives by free-knot regression splines, applied to the analysis of inner carotid artery centrelines. *J. R. Stat. Soc. Ser. C* 58:285–306, 2009.
- ³⁸Taylor, C. A., and D. A. Steinman. Image-based modeling of blood flow and vessel wall dynamics: applications, methods and future directions: sixth international bio-fluid mechanics symposium and workshop, March 28–30, 2008 Pasadena, California. *Ann. Biomed. Eng.* 38:1188–1203, 2010.
- ³⁹Timmins, L. H., D. S. Molony, P. Eshtehardi, M. C. McDaniel, J. N. Oshinski, D. P. Giddens, and H. Samady. Oscillatory wall shear stress is a dominant flow characteristic affecting lesion progression patterns and plaque vulnerability in patients with coronary artery disease. *J. R. Soc. Interface* 14:20160972, 2017.
- ⁴⁰Veneziani, A., and C. Vergara. Flow rate defective boundary conditions in haemodynamics simulations. *Int. J. Numer. Methods Fluids* 47:803–816, 2005.
- ⁴¹Zenonos, G., N. Lin, A. Kim, J. E. Kim, L. Governale, and R. M. Friedlander. Carotid endarterectomy with primary closure: analysis of outcomes and review of the literature. *Neurosurgery* 70:646–654, 2012; (discussion 654–645).

Publisher's Note Springer Nature remains neutral with regard to jurisdictional claims in published maps and institutional affiliations.